1.6 HIGH RESOLUTION SIMULATIONS OF THE ISLAND-INDUCED CIRCULATIONS FOR THE ISLAND OF HAWAII DURING HaRP

Yang Yang and Yi-Leng Chen*

Department of Meteorology
University of Hawaii at Manoa
Honolulu, Hawaii

1. Introduction

Mountains and hills affect the surface airflow and weather in several ways. Besides mechanically-forced ascent on the windward slopes, the mountains also act as a barrier to the approaching airflow and as a heat source (sink) during the day (night). In regions of complex terrain and various vegetation covers there are usually large gradients in wind, temperature, and moisture. Under these conditions, high resolution numerical guidance is required to assess the daily fire danger.

The island of Hawaii, roughly 140 km in diameters, is the largest island of the Hawaiian island chain. The topography is dominated by two volcanic mountains Mauna Loa and Mauna Kea, both of which exceed 4,100 m (Fig. 1), and extend well above the typical height of the trade-wind inversion (~ 2 km). In the past, comprehensive modeling studies were made by Nickerson (1979), Smolarkiewicz et al (1988) and Rasmussen et al (1989, 1993). These studies stress the airflow and cloud distributions from the effects of orographic lifting and island blocking. The island-induced diurnal circulations (Chen and Nash 1994) were not studied in sufficient detail in these studies.

Chen and Feng (2001) studied the effects of the trade wind inversion on the island-scale airflow and cloud distributions over the island of Hawaii with MM5v1 without considering the diurnal heating cycle. They found that in addition to the Froude number (Fr = U/Nh, where U is the upstream wind speed, N is the Brunt-Väsälä frequency, and h is the height of the barrier), the simulated island airflow and cloud distributions are sensitive to net diabatic heating associated with clouds and precipitation and rain evaporative cooling. Feng and Chen (2001) used the same model to study the nocturnal flow regime on the windward side of the island of Hawaii. Their results agree with observational studies. In their work, the land surface is specified as tropical rain forest everywhere. However, as pointed out in their paper, "large variations in local microclimate ranging from humid tropical climate on the windward slopes to hot desert over bare lava soils with different surface vegetation cover are typical for the Hawaiian Islands. To simulate the diurnal cycle, especially the surface thermal forcing during the day, an advanced land surface model with improved lower boundary conditions is needed."

* Corresponding author address: Prof. Yi-Leng Chen, Department of Meteorology, University of Hawaii, Honolulu, HI 96822; email: yileng@hawaii.edu

Recently, the Oregon State University land surface model (LSM) was incorporated into MM5 version 3 (Chen 2001). With the improved calculations of the surface latent and sensible heat fluxes, the MM5/LSM will be used to simulate the local circulations on the island of Hawaii during the full diurnal cycle. The dense observations from the PAM stations (Fig.1) and the upstream soundings from aircraft flight level data collected during the Hawaiian Rainband Project (HaRP) (11 July to 24 August, 1990) have been used to validate the MM5/LSM simulations over the entire island.

2. Model description and initialization

The MM5 (Duhia, 1993) is a nonhydrostatic, three-dimensional primitive equation model employing the terrain-following sigma vertical coordinate. In this study, there are 36 sigma levels from the surface to the 100-hPa level with 13 levels below sigma = 0.9. A two-way nesting procedure with four nested domains is used in this study with horizontal resolutions of 81 km, 27 km, 9 km and 3 km, respectively. The LSM incorporated in the MM5 has four layers underground: 10, 40, 100, and 200 cm. The land use and vegetation cover from the U.S. Geological Survey (USGS) 30 second resolution data were interpolated on the grid points of all domains.

The MM5 was initialized by NCEP/NCAR reanalysis data. Because of the low resolution of the data set (2.5º×2.5º), the soil moisture cannot be generated from the reanalysis data for the Hawaiian island chain. To solve this problem, MM5/LSM was run for two months prior to the HaRP period with the initial soil moisture specified according to the soil type and vegetation cover to generate the required soil moisture and soil temperature fields for HaRP simulations. Starting from 10 July, the simulation for each day during HaRP was initialized at 1200 UTC using the 24-h forecasts of the soil moistures and soil temperatures of the previous day and run for 48 hours. The output from the 12th hour and the 36th hour for each simulation were used to represent the simulated diurnal cycle of the following day.

3. The simulated winds

Fig. 2 shows the averaged winds from PAM observations (Fig. 2a) and the model simulation (Fig. 2b) for the entire HaRP period. The simulated winds were interpolated from the model output of the finest domain to the locations of PAM stations and are in good agreement with PAM observations. During HaRP, the mean upstream trade-wind speed from aircraft flight

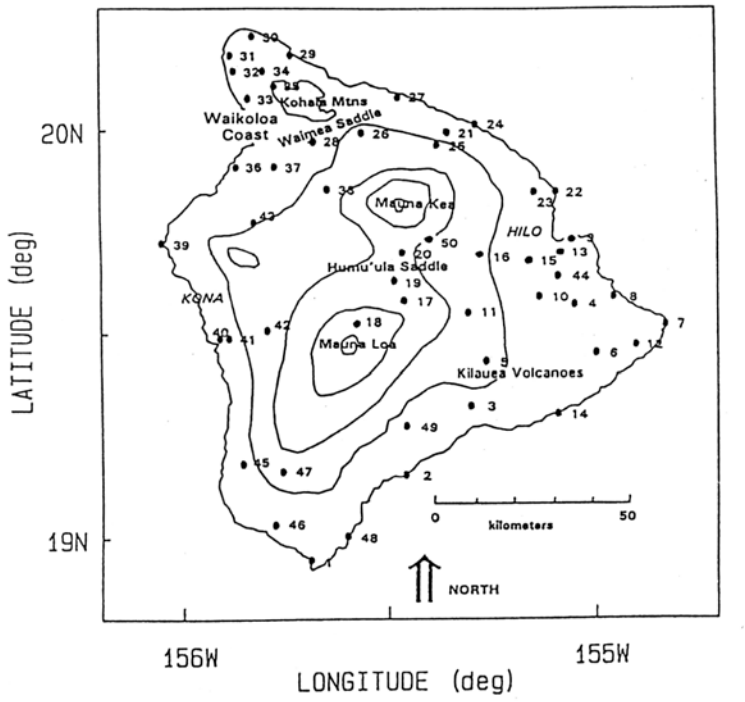

Figure 1. The island of Hawaii with PAM sites. Contours are for every 1000-m elevation

level observed data is about 6-8 m s^{-1} (Chen and Nash 1994). The weak winds in the Hilo Bay area and on the windward slopes as well as the splitting airflow along the windward coast as a result of island blocking are well simulated (Fig. 2). In addition to the northern and southern parts of the island, strong winds are also simulated in the Humu'ula Saddle between Mauna and Mauna Kea and in the Waimea Saddle (Fig. 2b). In the Kona area behind Mauna Loa and Mauna Kea, the trade-winds are completely blocked by the mountains with calm winds in the model simulations. These features are in agreement with observations (Fig. 2a). The main discrepancies between the simulated and observed mean winds occur over the northern and southern parts of the island and downstream of the Waimea Saddle (Fig. 2c). In these regions, the simulated winds are weaker than observed with differences in wind speed reaching as high as 3 m s^{-1}. Yang and Chen (2003) show that weaker trade wind strength upstream would result in smaller wind speed in these regions. It is apparent that the mean upstream trade-wind speed in the model is weaker than observations and is confirmed by a comparison between the observed and simulated upstream trade-wind soundings during HaRP. The simulated upstream trade-wind speed is ~1-3 m s^{-1} smaller than observations (not shown). Since the model is initialized by the NCEP/NCAR reanalysis, it appears the trade-wind strength in the vicinity of the island of Hawaii is underestimated by the reanalysis.

Both the daytime and nighttime flow regimes are well simulated by the model. The simulated surface airflow at 1400 HST (Fig. 3a, b) successfully reproduces the observed combined anabatic/trade-wind flow on the windward side, a splitting airflow with strong winds over the northern and southern tips, locally strong winds over Waimea Saddle and Humu'ulu, and sea breezes along the Kona coast. At 0200 HST katabatic/offshore flow is well simulated over most areas of the island except in regions with strong winds: the northern and southern tips, Waimea Saddle, and Humu'ulu Saddle (Fig. 3c, d).

However, some discrepancies exist between the simulated and observed winds. Similar to the mean winds over the entire HaRP period, the simulated trade-wind flow at the surface is 1-4 m s^{-1} smaller than observations over the southern tip, Kohala Mountains, and the leeside of Waimea Saddle for both the daytime and nighttime flow regimes. With a weaker incoming trade-wind flow in the model, the simulated katabatic flow over the eastern part of the island is 1-2 m s^{-1} greater than observations (Fig. 3c, d), reaching as high as 3 m s^{-1} at the eastern tip (Cape Kumukahi). On average, the offshore flow does not appear at Cape Kumukahi until 0400 HST (Chen and Nash, 1994), however, the simulated surface flow at 0200 HST exhibits offshore flow there. Furthermore, along the coast downstream of the Kohala Mountains, the nighttime offshore flow was not simulated.

For stations on the windward lowlands west of Hilo,

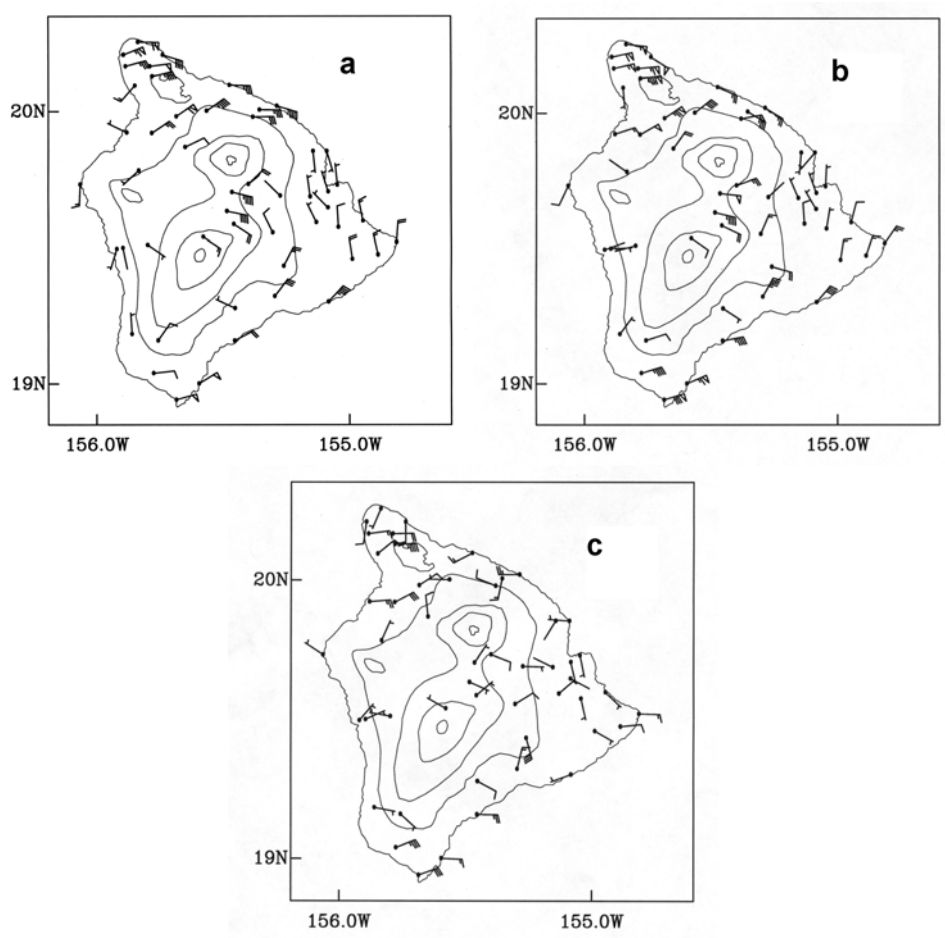

Figure 2. The daily average PAM wind during HaRP for (a) the simulation, (b) observations, and (c) vector of wind difference between (a) and (b). Pennants, full barbs, and half barbs represent 5, 1, and 0.5 m s^{-1} respectively (the same hereafter).

the evolution of diurnal winds is well simulated (Fig. 4). The timing of the turning of the winds from downslope (upslope) to upslope (downslope) during the morning (evening) transition agrees with observations reasonably well.

For the Kona area on the leeside of the island, the morning transition from downslope flow to upslope flow was well simulated (~ 0800 HST) (not shown). The evening transition at the Kona coast is also well simulated. However, on the Kona slope, the simulated evening transition from upslope flow to downslope flow was 2 - 4 hours later than observations.

4. **The simulated surface temperature**

The terrain height of the model is not exactly the same as that of the real terrain. In order to reduce the effect of the model terrain height error on the temperature difference between the model prediction and observations, the simulated temperature deviation at each grid point is computed by subtracting the temperature of the mean upstream at the same level from the simulated grid point temperature. Then the grid point temperature deviations were interpolated to the locations of PAM stations. At each PAM station, the observed temperature deviation from the same upstream mean sounding at the same level was also calculated.

The simulated diurnal temperature ranges are in good agreement with observations with a few exceptions. The surface thermal fields are not only controlled by the diurnal heating cycle but also by the airflow and the distributions of clouds and rains (Chen and Wang, 1995). A weaker trade wind flow would result in weaker adiabatic descent in the leeside areas where the mountain ridges is lower than 2 km (Yang and Chen, 1993). These areas include: the lee-side area of the Kilauea Volcanoes, southwestern corner and the leeside area downstream of the Waimea Saddle. Since the simulated upstream trade-wind strength is weaker than observed, the adiabatic warming in these areas is underestimated (Fig. 5). During the daytime, the simulated surface temperature deviations in these areas are 2-4^{o} C lower than observed (Fig. 5a, b). In the early morning, the negative temperature deviations in these areas are about 1^{o} C larger (Fig. 5c, d).

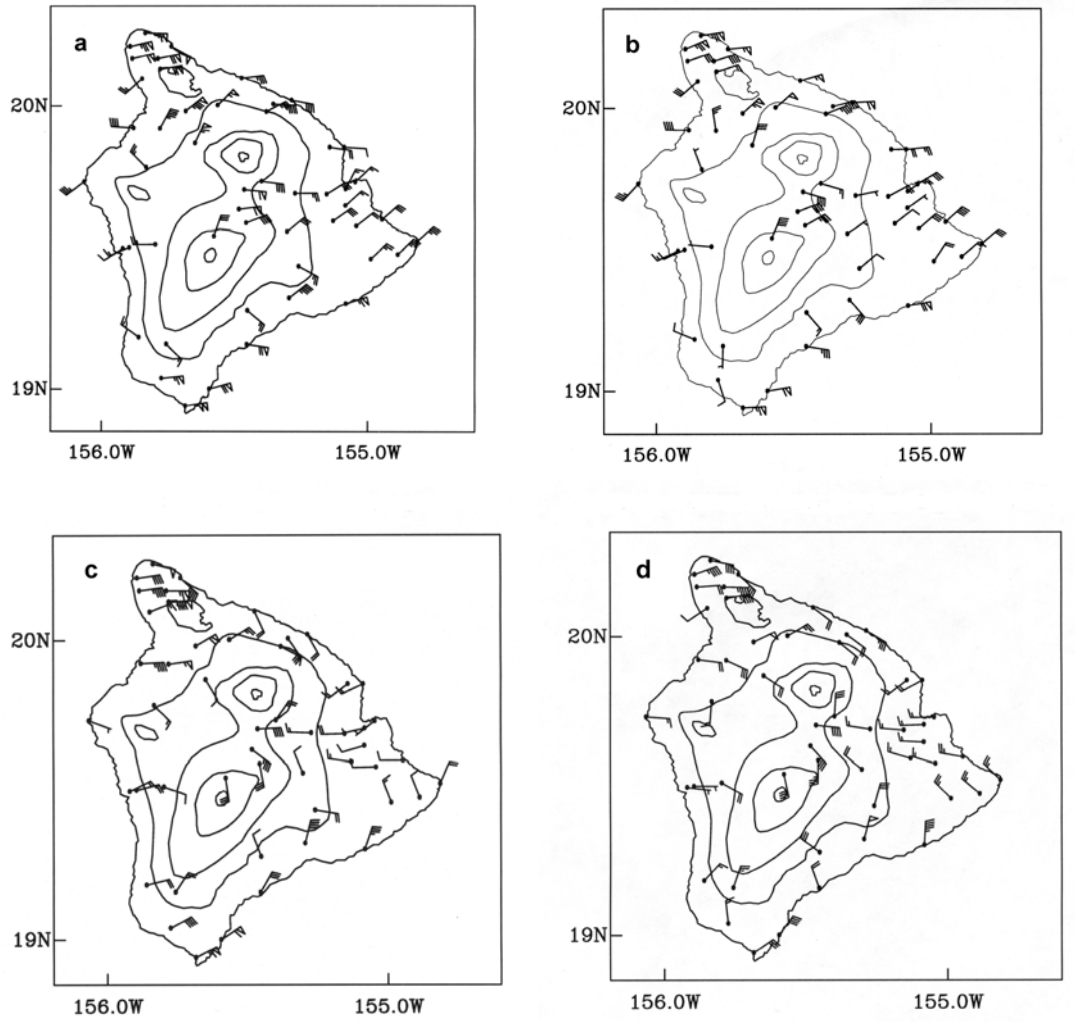

Figure 3. The average PAM wind vector during HaRP at 1400 HST for (a) observations and (b) the simulation, and at 0200 HST for (c) observations and (d) the simulation.

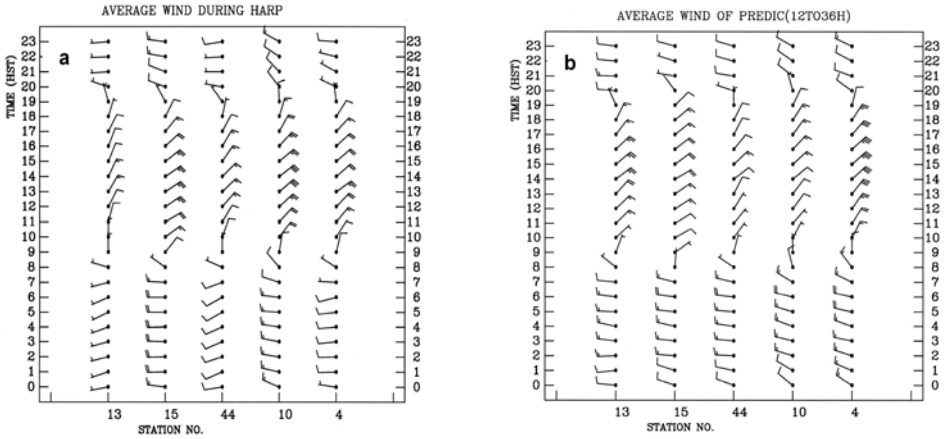

Figure 4. The average wind vectors during HaRP throughout the diurnal cycle at stations 13, 15, 44, 10, and 4 on the windward lowlands west of Hilo for (a) observations and (b) the simulation.

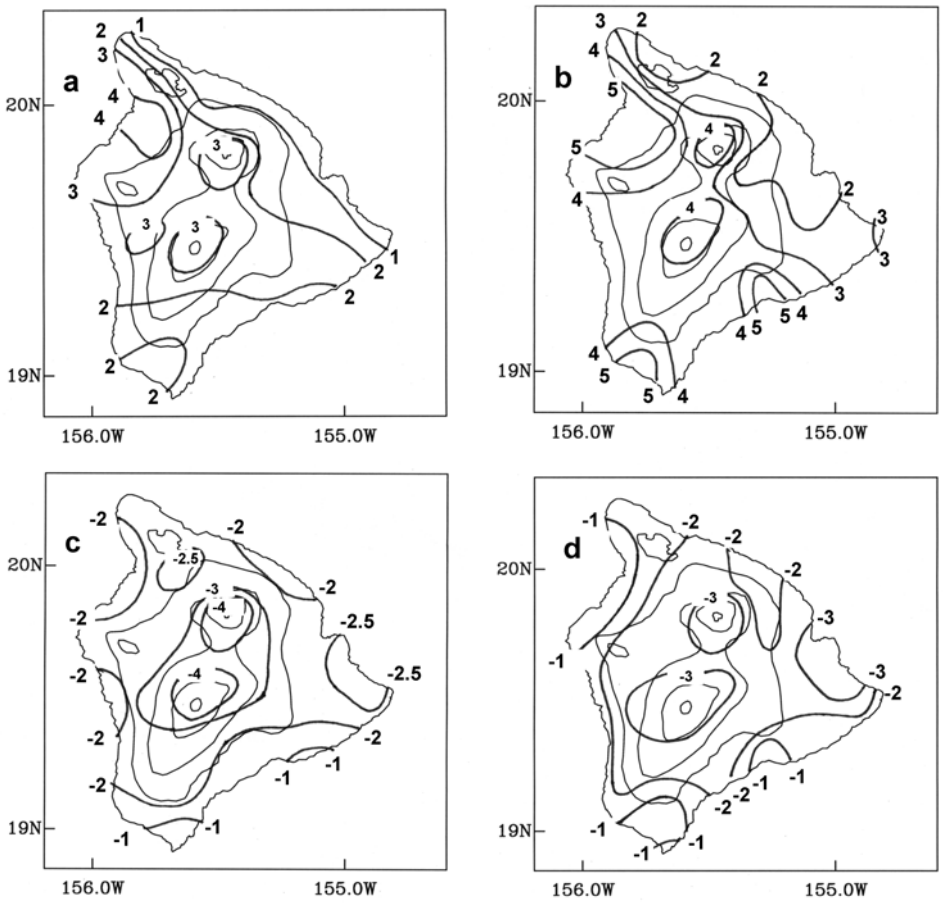

Figure 5. The temperature deviations from the upstream environment at the same height for (a) the simulation and (b) observations at 1400 HST, and for (c) the simulation and (d) observations at 0500 HST.

On the windward side, at 1400 HST, the observed mean temperature deviations are in the range of 1.5-3^{o} C, which is considerably smaller than the observed temperature deviations in the lee areas (4-6^{o} C) (Fig. 5a, b). The simulated diurnal temperature perturbation on the windward side is slightly smaller than observed. In the early morning, over the windward side lowlands and the Hilo coastal areas, the simulated negative temperature deviations are ~1^{o} C smaller than observations (Fig. 5c, d) but with a stronger katabatic/offshore flow (Fig. 3d). It is apparent that the excessively strong simulated katabatic flow in the region is related to the weaker in-coming trade-wind flow in the model. The katabatic flow is better developed with a weaker incoming trade-wind flow even though the negative temperature deviations are smaller there. It is interesting to note that the simulated temperature deviations on the upper slopes are larger in the model simulations. With clear skies on the upper slopes in the early morning, the lower temperatures on the upper slopes are mainly related to radiative cooling. In the coastal areas, rain evaporative cooling is also important (Feng and Chen 2001). The smaller negative temperature deviations in the model at lower elevations may be related to smaller evaporative cooling with less rainfall in the model as will be shown in the next section.

5. Predicted rainfall on the island of Hawaii

The simulated total rainfall accumulation for the entire HaRP suggests that most of the rainfall occurs on the windward side of the island (Fig. 6a). On the lee side, the simulated rainfall accumulation is much less except in the Kona region. The driest areas are found over the summits of Mauna Loa and Mauna Kea, northwestern Hawaii, downstream of Waimea Saddle, southwestern Hawaii, and along the southeastern coast. These results are in general agreement with observations (Fig. 6b). However, some discrepancies exist between the simulated and observed rainfall accumulation. On the windward side, the simulated maximum rainfall axis (~ 490 mm) is along the coast whereas the observed maximum rainfall accumulation (~ 600 mm) is over the windward lowlands west of Hilo. The simulated maximum rainfall accumulation on the windward side of the Kohala Mountains is ~ 200 mm which is considerably less than the observed rainfall

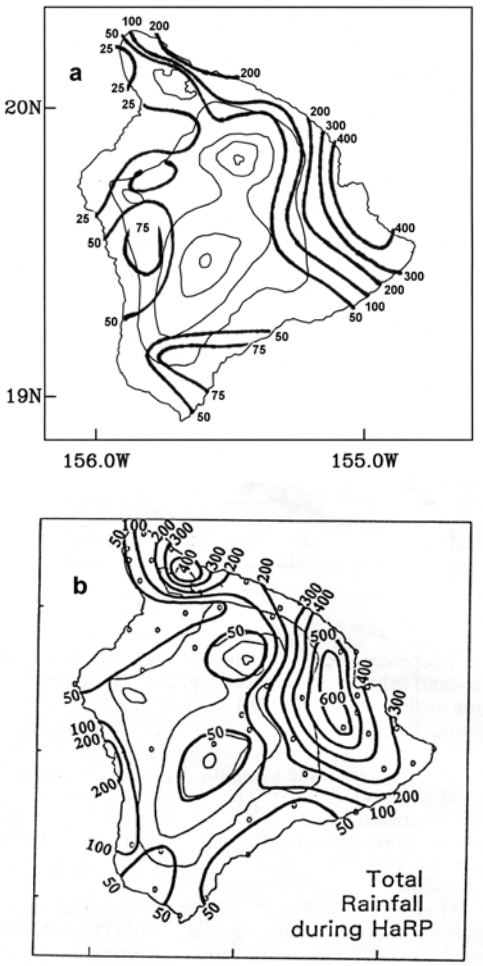

Figure 6. The total rainfall accumulation (mm) during HaRP for (a) the simulation and (b) observations.

accumulation (~ 400m) there. In the Kona area, the observed rainfall maximum (~200 mm) is along the coast whereas the simulated rainfall maximum (~ 75 mm) is on the lower Kona slopes.

Aside from the model bias itself, the uncertainties in the initial conditions affect the model results. The weak upstream trade-wind speed contributes to the errors in the values and locations of maximum simulated rainfall accumulations significantly. The orographic lifting on the windward side is weaker with less rainfall when the incoming trade-wind flow is weaker (Esteban and Chen 2003). On the lee-side the return flow off the Kona coast as a result of island blocking will also be weaker (Yang and Chen 2003). In addition to dynamic effects, a weaker trade-wind flow would also affect the rainfall as a result of complex interactions among orographic lifting, island blocking and thermally induced circulations both on the windward side and the lee side (Esteban and Chen 2003; Yang and Chen 2003) Chen and Feng (1995) show that the maximum rainfall west of Hilo mainly occurs around midnight due to the convergence between the katabatic flow and the incoming trade-wind flow and enhanced by orographic lifting aloft. The location of this convergence zone is affected by the upstream strength (Esteban and Chen 2003). When trades are weaker, the convergence zone moves toward the coast with much less rainfall over the windward lowlands. Yang and Chen (2003) suggest that the maximum rainfall along the Kona coast in the evening is caused by the convergence between the dynamically-driven return flow offshore and the land breezes. Under weaker trades, the rainfall there is much less (Yang and Chen 2003). Further studies on the effects of trade-wind strength on the rainfall production during different time of the day will be made based on model sensitive tests. Furthermore, the pre-existing trade-wind clouds and showers may drift inland and produce localized trade-wind showers as they interact with the island induced circulations (Austin et al, 1986; Frye and Chen 2001). The pre-existing trade-wind cloud fields are not included in the initial conditions.

6. Summary

Overall, the island blocking, orographic lifting, and the diurnal cycles of the surface winds, temperature and rainfall over the Island of Hawaii are well simulated. The simulated splitting airflow, strong winds over the northern and southern tips, Waimea Saddle, and Humu'ulu Saddle of the island of Hawaii are in good agreement with observations. At most areas on the windward side and the Kona coast on the leeside, the upslope (downslope) flow duration and the morning (evening) transition time from downslope (upslope) flow to upslope (downslope) agree well with observations. The simulated diurnal temperatures are generally in good agreements with observations. The surface temperature is better simulated on the windward side than the leeside, and during the nighttime than during the daytime. The distribution of rainfall accumulation on the island is similar to observations with more rainfall on the windward side and much less rainfall over the summits of Mauna Loa and Mauna Kea, northwestern Hawaii, downstream of Waimea Saddle, southwestern Hawaii, and along the southeastern coast.

The simulated winds are smaller than observations over the southern and northern parts of the island and downstream of the Waimea Saddle with wind speed difference up to 4 m s^{-1}. During the daytime the simulated surface temperatures on the island are generally lower than observations with large differences (2-4º C) on the leeside area of the Kilauea Volcanoes, southwestern corner and the leeside area downstream of the Waimea Saddle. In the early morning, the negative temperature deviations in these areas are about 1º C larger. On the windward side, the simulated maximum rainfall axis (~490 mm) is along the coast whereas the observed maximum rainfall accumulation (~600 mm) is over the windward lowlands west of Hilo. On the windward side of Kohala Mountains and the Kona coast on the leeside, the simulated maximum rainfall is ~50% smaller than observation.

Most of the discrepancy between the simulation and observations can be attributed to the weaker trade wind flow upstream (1~3 m s^{-1} difference) simulated in the model. Since the model is initialized by the NCEP/NCAR reanalysis, it appears the trade-wind strength in the vicinity of the island of Hawaii is underestimated by the reanalysis. With weaker trade wind flow, the winds over the southern part of the island, downstream of the Waimea Saddle are smaller. The adiabatic warming caused by the descent of trade wind flow on the leeside area of Kilauea Volcanoes, southwestern corner and leeside area downstream of the Waimea Saddle are also smaller, and cause cooler simulated temperature in these areas.

When trade wind flow is weaker, the convergence zone between the Katabatic flow and the incoming trade-wind flow moves toward the coast with much less rainfall over the windward lowlands. Along the Kona coast, the evening maximum rainfall is caused by the convergence between the dynamically driven return flow offshore and the land breeze. Under weaker trades, the return flow is weaker; as a result, less rain falls.

The pre-existing trade-wind cloud fields frequently observed upstream are not included in the initial conditions, which can produce localized trade-wind showers as they interact with the island induced circulations and affect the surface temperature through evaporation cooling and cloud radiation feedback effects.

Acknowledgement

This work is supported by the National Science Foundation under Grant ATM-0140387 and the US Forest Service under cooperative agreements 01-CA-11272169-146 and 03-CA-11272169-305. We thank B. Kerns for reading the text.

Reference

Austin, G. R., R. M. Rauber, H. T. Ochs III, and L. J. Miller, 1986: Trade-wind clouds and Hawaiian rainbands. *Mon. Wea. Rev.*, **124**, 2126-2151.

Chen, F., and J. Dudhia, 2001: Coupling an advanced land surface-hydrology model with the Penn State-NCAR MM5 modeling system. Part II: Preliminary Model Validation. *Mon. Wea. Rev.,* **129,** 587-604.

Chen, Y. L., and J. Feng, 2001: Numerical simulations of airflow and cloud distributions over the windward side of the island of Hawaii. Part I: The effects of trade wind inversion, *Mon. Wea. Rev.,* **129**, 1117-1134.

-----, and J.-J. Wang, 1995: The effects of precipitation on the surface temperature and airflow over the island of Hawaii. *Mon. Wea. Rev.*, **123**, 681-694.

-----, and A. J. Nash, 1994: Diurnal variations of surface airflow and rainfall frequencies on the island of Hawaii. *Mon. Wea. Rev*., **122**, 34-56.

Dudhia, J. (1993): A nonhydrostatic version of the Penn state-NCAR mesoscale model: validation tests and simulation of an Atlantic cyclone and cold front. *Mon. Rea. Rev.*, **121**, 1493-1513.

Esteban, M. A., and Y.–L. Chen, 2003: The impact of trade-wind strength on precipitation over the windward side of the island of Hawaii. *Mon. Wea. Rev*., in review.

Feng, J., and Y. L. Chen, 2001: Numerical simulations of airflow and cloud distributions over the windward side of the island of Hawaii. Part II: Nocturnal flow regime, *Mon. Wea. Rev*., **129,** 1135-1147.

Frye, J., and Y.-L. Chen, 2001: Evolution of downslope flow under strong opposing trade winds and frequent trade-wind rainshowers over the island of Hawaii. *Mon. Wea. Rev*., **129**, 956-977.

Nickerson, E. C., 1979: On the numerical simulation of airflow and clouds over mountainous terrain. *Beitr. Phys. Atmos*., **52**, 161-175.

Rasmussen, R. M., and P. K. Smolarkiewicz, 1993: On the dynamics of Hawaiian cloud bands. Part III: local aspects*, J. Atmos. Sci.*, **50**, 1560-1572.

------, and J. Warner, 1989: On the dynamics of Hawaiian cloud bands: comparison of model

results with observations and island climatology. *J. Atmos. Sci*., **46**, 1589-1608.

Smolarkiewicz, P.K., R. M. Rasmussen, and T. L. Clark, 1998: On the dynamics of Hawaiian cloud bands: Island forcing, *J. Atmos. Sci*., **45**, 1872-1905.

Yang, Y., and Y.-L. Chen, 2003: Circulations and rainfall on the leeside of the island of Hawaii during HaRP. *Mon. Wea. Rev*., **131,** 2525-2542.